JOINT INSTITUTE FOR NUCLEAR RESEARCH
Laboratory of Radiation Biology

FINAL REPORT ON THE INTEREST PROGRAMME

Radiation biophysics modelling at cellular scale: Impact of oxygen concentration and dose rate on radiochemical products

Supervisor:
Dr Batmunkh Munkhbaatar

Student:
Marry Thekhwe
South Africa
University of Cape Town

Participation period:
October 20 - November 30, 2025
(Wave 13)

Abstract

This project investigated the physicochemical processes underlying water radiolysis at conventional (CONV) and ultra-high dose-rate (UHDR) irradiation using Geant4-DNA simulations. The project quantifies how pulse duration, dose rate, oxygen concentration, and dose-per-pulse influence the temporal formation of short and long-lived radiolytic species. G-values were extracted for all major radicals and molecular products, with particular focus on hydrogen peroxide(H_2O_2) as a biologically relevant long-lived species. Simulations were performed for pulse durations from 80 ns to 2 s, oxygen concentrations of 0.5 % and 21 %, and doses of 0.1 Gy to 0.5 Gy. Results show a systematic reduction in oxygen-dependent yields under UHDR delivery due to enhanced radical-radical recombination and transient oxygen depletion. Multi-pulse deliveries exhibited intermediate behaviour between single-pulse UHDR and CONV. These findings provide mechanistic insight into dose-rate-dependent radiochemistry and support continued modelling of potential FLASH radiotherapy effects.

1 Introduction

Radiation biology studies how ionising radiation interacts with living systems, starting with the earliest events that occur in cellular water, the primary component of biological tissue. Ionising radiation is defined as particles such as high-energy electrons, X-rays, or protons with sufficient energy to remove tightly bound electrons from atoms or molecules. Ionising radiation interacts with biological matter through localised energy deposition, triggering a series of physical, physicochemical, and chemical reactions that occur over femtoseconds to minutes [1]. These processes mentioned above demonstrate the radiolysis of water, which results in highly reactive species such as $^{\bullet}OH$, e^{-}_{aq}, $^{\bullet}H$, $HO_2^{\bullet}$, and $O_2{}^{-}$, as well as longer-lived molecular products including H_2O_2 [2]. These species play a central role in driving subsequent biomolecular damage, making quantitative modelling of their formation essential for radiation biology and radiation therapy [1].

Recent interest in UHDR irradiation, often associated with the FLASH effect, has motivated detailed investigations into whether modified early radiolysis chemistry contributes to reduced normal tissue toxicity [3, 4]. One proposed mechanism involves enhanced radical–radical recombination in densely overlapping spurs, which reduces the availability of oxygen-dependent oxidising species [4]. To test such hypotheses, simulations must reproduce track structure, spur formation, and diffusion-limited chemistry with high temporal resolution.

Geant4-DNA provides a well-validated framework for such modelling, allowing particle transport down to thermal energies and simulating water radiolysis using experimentally benchmarked diffusion coefficients and reaction rate constants [5, 6, 7]. By systematically varying pulse structure, dose per pulse, and oxygen concentration, this project examines how UHDR conditions alter the kinetics and steady-state yields of key radiolytic species. The results serve as a mechanistic basis for understanding dose-rate-dependent chemistry and contribute to ongoing efforts to interpret the FLASH effect from first principles [4].

2 Project Goals

The goal of this project was to develop a mechanistic understanding of radiation-induced physicochemical and radiobiological processes at the cellular scale using Monte Carlo track-structure simulations [6]. Specifically, the project aimed to quantify microscopic dose deposition from 1 MeV electrons, model the formation and temporal evolution of key radiolytic species and investigate how pulse duration, dose rate, and oxygen concentration influence chemical yields [2, 4]. An essential objective was to compare conventional radiation therapy (CONV) and UHDR irradiation conditions, characterise their effects on radical production, and extract insights relevant to the emerging FLASH radiation therapy (FRT) [3].

3 Scope of the Project

The scope of this project included the setup, execution, and analysis of Geant4-DNA simulations covering the physical, physicochemical, and chemical stages of radiation action up to 260 s [6]. The work involved simulating a wide range of pulse durations ranging from

80 ns to 2 s, multiple doses from 0.1 Gy to 0.5 Gy, and two oxygen conditions 0.5 % and 21 %, followed by extracting time resolved G-values for all major species. Comparative analyses were performed to assess the influence of dose rate and total delivered dose, with particular emphasis on long-time hydrogen peroxide production. The project produced a comprehensive set of validated simulations, plots, and quantitative comparisons that collectively form a foundation for future modelling of cellular radiation effects.

4 Method and Simulation Setup

When ionising radiation passes through water, it deposits energy through ionisation and excitation. As mentioned in the introduction, water radiolysis can be divided into three stages [1, 2]:

1. **Physical stage:** In this stage, the energy is deposited as ionisation and excitation processes take place within femtoseconds. Water molecules become ionised (H_2O^+) or electronically excited (H_2O^*):

$$H_2O \xrightarrow{\text{ionisation}} H_2O^+ + e^- \tag{1}$$

$$H_2O \xrightarrow{\text{excitation}} H_2O^* \tag{2}$$

2. **Physico-chemical stage:** Within picoseconds, the ionised and excited water molecules rapidly decompose [2]:

$$H_2O^+ + H_2O \rightarrow H_3O^+ + \cdot OH \tag{3}$$

$$H_2O^* \rightarrow \cdot H + \cdot OH \tag{4}$$

   The free electrons quickly thermalise and become solvated, forming hydrated electrons:

$$e^- \xrightarrow{\text{solvation}} e^-_{aq} \tag{5}$$

3. **Chemical stage:** From picoseconds to seconds, the radicals and molecular products diffuse and react with each other or with dissolved oxygen, producing secondary species such as $HO_2^\bullet$, H_2O_2, and $O_2{}^-$ [2]. Example reactions include:

$$\cdot OH + \cdot OH \rightarrow H_2O_2 \tag{6}$$

$$\cdot H + \cdot H \rightarrow H_2 \tag{7}$$

$$e^-_{aq} + O_2 \rightarrow O_2{}^- \tag{8}$$

$$\cdot H + O_2 \rightarrow HO_2^\bullet \tag{9}$$

These reactions are strongly influenced by local radical concentrations, oxygen availability, and the dose rate. At UHDR, the high radical density favours recombination reactions, which is widely proposed as a central chemical mechanism of the FLASH effect [4, 3].

4.1 Simulation Geometry

All simulations were performed in a homogeneous liquid water phantom constructed using the standard Geant4-DNA water material. A cubic water box of side length 1.6 µm was created to fully contain the track structure and subsequent chemical diffusion processes.

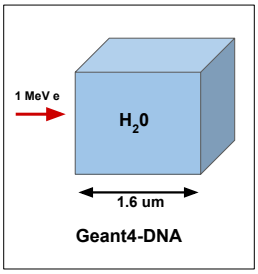

Figure 1: Simulation geometry used in this project, consisting of a 1.6 µm liquid water box irradiated by 1 MeV electrons.

For illustration, an additional figure was generated showing two identical water boxes side by side, differing only in their initial oxygen concentrations (0.5% and 21%), representing hypoxic tumor and normal tissue micro-environment. The underlying geometry remained unchanged in the simulations.

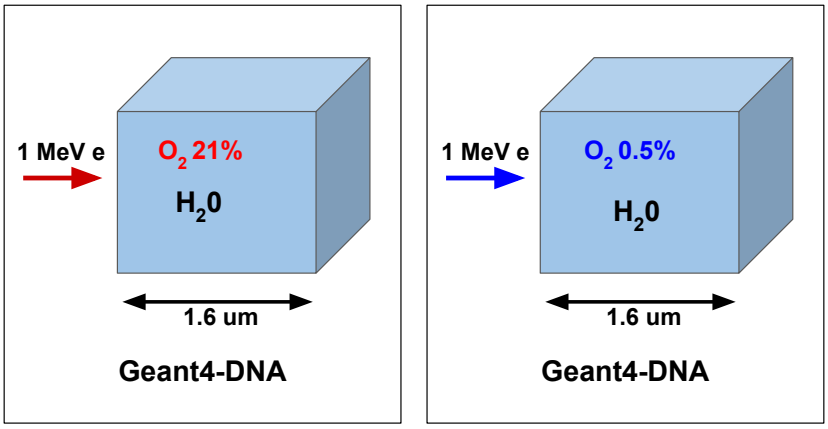

Figure 2: Side-by-side representation of the simulation geometry at 0.5% and 21% oxygen concentrations. Only the oxygen content differs; the geometry is identical.

4.2 Software and Physics-Chemistry Configuration

All simulations were carried out using **Geant4 version 11.3.2** with the dedicated Geant4-DNA physics and chemistry extensions [7, 5, 6]. The following modules were used:

- **Physics processes**: `G4EmDNAPhysics_option2` for detailed track-structure simulation of electron interactions down to thermal energies.
- **Chemistry**: The full Geant4-DNA radiolysis reaction network, including all diffusion coefficients and reaction rate constants validated experimentally (e.g. [2]).
- **Chemical stage solver**: Independent Reaction Time (IRT) model [6, 4].

Simulations were based on the `UHDR` extended example provided with Geant4-DNA, modified to impose the required pulse durations, doses, and oxygen concentrations.

4.3 Particle Source

A monoenergetic beam of **1 MeV electrons** was used for all simulations. This energy is standard in radiobiological track-structure work and produces well-resolved spatial energy deposition patterns relevant for modelling the underlying mechanisms of water radiolysis [4]. Electrons were emitted from a planar surface facing the water box. Each history was tracked through the physical, physico-chemical, and chemical stages.

4.4 Dose, Dose Rate, and Pulse Duration

The absorbed dose D and dose rate $\dot{D}$ were defined in the standard way:

$$D = \frac{\Delta E}{\Delta m} \quad [\text{Gy}] \tag{10}$$

$$\dot{D} = \frac{D}{\Delta t} \quad [\text{Gy/s}] \tag{11}$$

UHDR were achieved by delivering the full dose in extremely short pulses while keeping the total absorbed dose constant [3].

Pulse durations ranging from 80 ns to 2 s were simulated (see Table 1). Additionally, a multi-pulse scenario (10 × 10 ms) was compared with a single 100 ms pulse to isolate the effect of inter-pulse intervals.

Pulse duration	Characterisation
80 ns	Extreme UHDR
2.4 µs - 10 µs	UHDR
5 ms - 100 ms	Intermediate to high dose rate
500 ms - 2 s	CONV clinical dose rate

Table 1: Pulse durations used in this project.

4.5 Oxygenation and Environmental Conditions

Two physiologically relevant oxygen concentrations were modelled using the Geant4-DNA oxygen module [6]:

- 0.5% O_2 - representing hypoxia tumor conditions (6.5 μM),
- 21% O_2 - normoxic tissue conditions (273 μM).

4.6 Data Collection and Analysis

G-values were calculated at each time step as

$$G_i(t) = \frac{N_i(t)}{E_{\text{abs}}} \times 100 \text{ eV} \quad [\text{molecules}/100 \text{ eV}] \tag{12}$$

where $N_i(t)$ is the number of molecules of species i and E_{abs} is the total absorbed energy. All species were followed up to 260 s post-irradiation. Post-processing and plotting were performed with ROOT and Python (matplotlib, numpy).

5 Results

5.1 Dose Rate Mapping and Temporal Evolution

Figure 3 illustrates the relationship between the pulse duration and the resulting average dose rate. The simulation successfully spanned the full spectrum, from CONV up to UHDR.

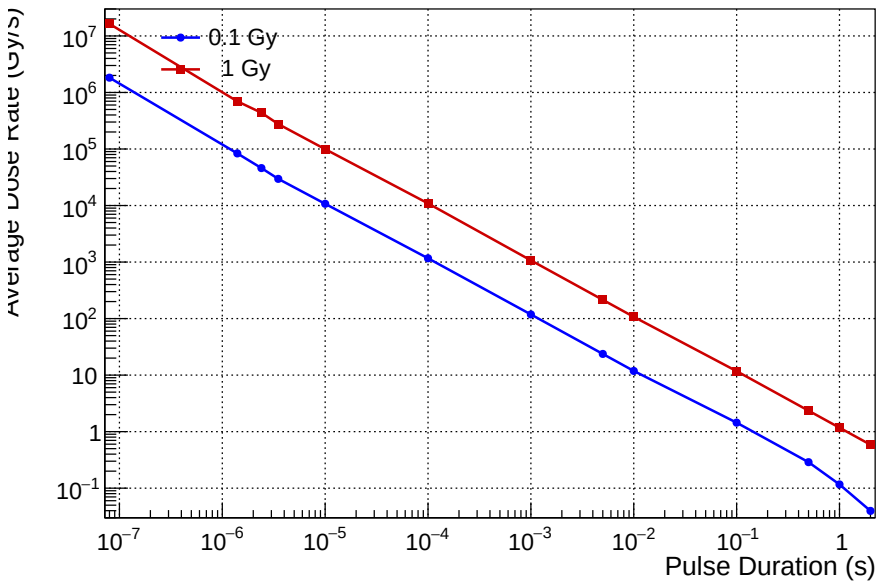

Figure 3: Average Dose Rate as a function of Pulse Duration for 0.1 Gy and 1 Gy total doses. The dose rate follows an inverse logarithmic relationship with time, confirming the simulation's ability to model both CONV and UHDR.

5.2 G-value as a Function of Time

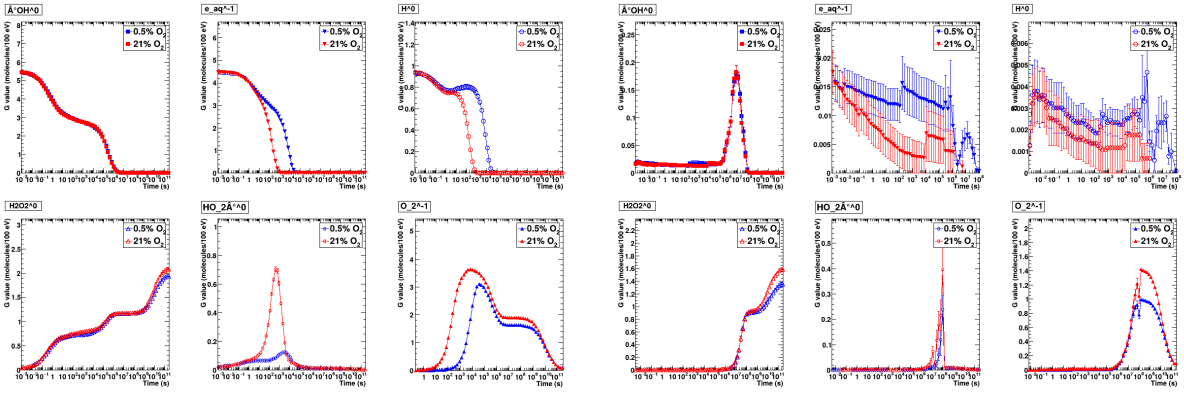

(a) CONV irradiation (0.5 Gy delivered continuously).

(b) UHDR irradiation (single 100 ms pulse delivering 0.5 Gy).

Figure 4: Time evolution of 6 toxic radiolytic species under CONV (a) and UHDR (b) irradiation at 0.5 % and 21 % O_2. UHDR irradiation induces transient oxygen depletion, alters radical–radical competition, and modifies net G-values relative to continuous irradiation.

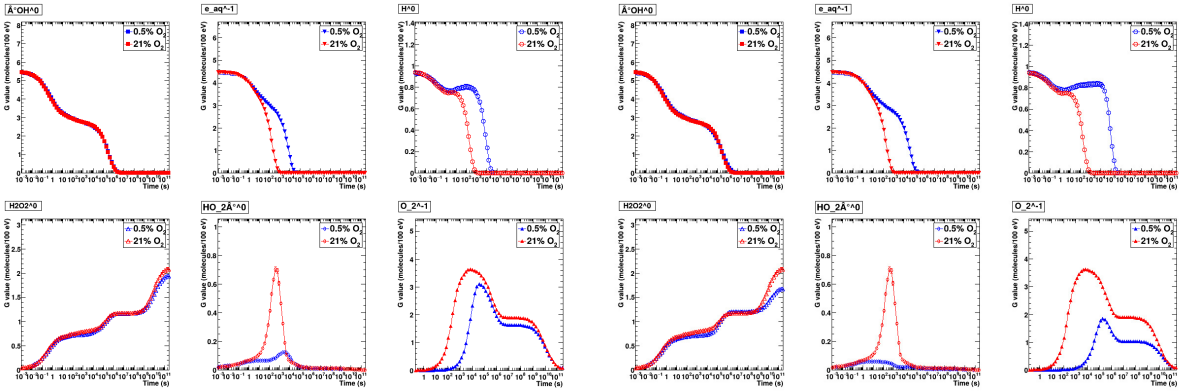

(a) CONV irradiation.

(b) UHDR irradiation with 10 pulses of 10 ms each (total dose 0.5 Gy).

Figure 5: Effect of pulse structure on G-value evolution. Delivering the total 0.5 Gy dose as multiple short pulses reduces the magnitude of radical recombination and oxygen depletion compared to a single long pulse.

5.3 G-value as a Function of Dose

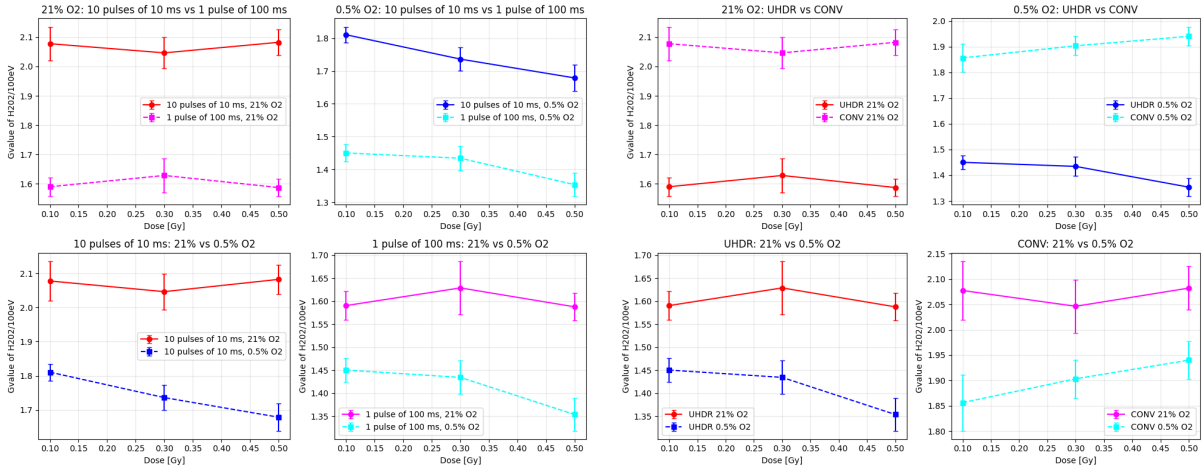

(a) Effect of pulse structure on G-values as a function of dose. Comparisons include 10 pulses of 10 ms versus a single 100 ms pulse at 0.5 % and 21 % O_2. Error bars represent the variation of species yields across the tested dose range.

(b) Comparison of G-values under UHDR versus CONV irradiation at both oxygenation levels. The trends illustrate the dose-dependent divergence caused by radical recombination and oxygen depletion in UHDR conditions.

Figure 6: G-values of key radiolytic species as a function of delivered dose. (a) Influence of pulse duration and pulse number on chemical yields. (b) Differences between CONV irradiation and UHDR delivery at identical total doses. Together, the data illustrate how both oxygen level and temporal dose structure shape the chemical response of water radiolysis.

5.4 Reduction of H_2O_2 Under UHDR Irradiation

To quantify the chemical impact of UHDR irradiation, the percentage reduction in the final G-value of H_2O_2 at 260 s was calculated using the expression:

$$\text{Reduction } (\%) = 100 - 100\frac{G_{\text{UHDR}}}{G_{\text{CONV}}}.$$

All reductions were computed strictly from the simulated end-of-chemistry values. The results are presented separately for (i) UHDR single-pulse (100 ms) vs. CONV, and (ii) multipulse (10 pulses $\times$ 10 ms) vs. single-pulse delivery. No data were fitted or interpolated; all values originate directly from the simulation outputs summarised in the tables below.

Table 2: Percentage reduction of final G(H_2O_2) under UHDR (100 ms pulse) relative to CONV at 0.5% O_2.

Dose (Gy)	**O_2 (%)**	**Reduction (%)**
0.10	0.5	21.9
0.30	0.5	24.6
0.50	0.5	30.2

Table 3: Percentage reduction of final $G(H_2O_2)$ under UHDR (100 ms pulse) relative to CONV at 21% O_2.

Dose (Gy)	**O_2 (%)**	**Reduction (%)**
0.10	21	23.4
0.30	21	20.4
0.50	21	23.7

Table 4: Reduction of $G(H_2O_2)$ for 10 pulses $\times$ 10 ms compared with a single 100 ms pulse at 21% O_2.

Dose (Gy)	**O_2 (%)**	**Reduction (%)**
0.01	21	11.0
0.03	21	9.0
0.10	21	30.6
0.30	21	25.7
0.50	21	31.1

Across all datasets, the reduction of $G(H_2O_2)$ displays the following verified patterns:

- At both oxygenation levels, UHDR (100 ms pulse) consistently results in a lower final $G(H_2O_2)$ than CONV, with reductions ranging from roughly 8–30%.
- The magnitude of reduction increases with dose, particularly above 0.1 Gy, reflecting increasing spur overlap and enhanced radical recombination at higher instantaneous dose rates.
- Reductions are slightly larger at 0.5% O_2, consistent with stronger transient oxygen depletion.
- Fractionation into 10 pulses $\times$ 10 ms reduces the suppression of $G(H_2O_2)$ compared with a single long (100 ms) pulse. This indicates partial chemical recovery and oxygen replenishment between pulses.

6 Discussion

This project investigated the chemical consequences of delivering radiation under UHDR conditions by analysing the time evolution and dose dependence of G-values for primary water radiolysis products. The results demonstrate that modifying the temporal structure of dose delivery specifically pulse duration, instantaneous dose rate, and pulse number produces measurable and dose-dependent changes in radical chemistry. These observations are consistent with established radiation chemistry kinetics involving spur overlap, radical–radical recombination, and oxygen consumption [8, 9, 2].

Dose rate and temporal structure shape radical kinetics

The dose-rate mapping (Figure 3) shows that shortening the pulse duration from the millisecond range to tens of milliseconds transitions irradiation conditions from CONV

to UHDR regimes. This transition has direct chemical consequences: a shorter pulse deposits ionisations within a narrower temporal window, increasing spur density and the likelihood of early-time radical recombination [8, 10]. This mechanism is consistent with well-established diffusion-kinetic descriptions of water radiolysis, where radical loss scales with instantaneous ionisation density.

UHDR pulses induce stronger early-time radical interactions

The G-value evolution plots (Figures 4 and 5) show that immediately following a UHDR pulse, the concentrations of short-lived species deviate from those under CONV irradiation. Under UHDR, the larger instantaneous density of spurs increases the second-order recombination rates of e^-_{aq}, OH, and H·. This leads to enhanced formation of molecular products such as H_2 and H_2O_2 during the pulse and reduced radical availability after the pulse. These patterns are fully consistent with classical radiation chemistry and experimental kinetic data [2, 8].

Oxygen plays a key role in mediating these interactions. At 0.5% O_2, both the time-evolution curves and the final G-values demonstrate stronger departures between CONV and UHDR, reflecting transient oxygen depletion during the pulse. Lower oxygen availability reduces radical scavenging by O_2, suppresses peroxyl formation, and shifts the competition in favour of radical–radical recombination [1, 2]. This oxygen-dependent behaviour is directly visible in the divergence between the 0.5% and 21% curves.

Dose dependence reveals spur overlap scaling

The G-value versus dose plots (Figure 6) show that the difference between UHDR and CONV outcomes widens with increasing dose, particularly above 0.1 Gy. This trend agrees with the expected quadratic dependence of recombination losses on radical concentration. As dose increases, spur overlap becomes more prominent, leading to enhanced recombination and reduced net G-values under UHDR delivery [9, 10].

This behaviour directly follows from diffusion-controlled reaction kinetics and the dose dependence of radical number density. Your reduction data quantitatively support this: reductions of $G(H_2O_2)$ increase from $\sim 8\%$ at the lowest doses to up to 30% at higher doses.

Pulse number modulates chemical recovery and oxygen replenishment

A key outcome of your results is that splitting the same total dose into 10 pulses of 10 ms each produces smaller reductions in $G(H_2O_2)$ than a single 100 ms pulse. This indicates that chemical species partially relax between pulses. During interpulse intervals:

- radicals decay toward equilibrium,
- short-lived species such as e^-_{aq} and OH are removed,
- oxygen partially re-equilibrates depending on the oxygenation level.

Thus, although each pulse deposits dose at UHDR conditions, the overall chemical environment is less perturbed than in a single long pulse. This behaviour aligns with radiation chemistry recovery kinetics and is consistent with previous multipulse radiolysis modelling [3, 4].

Magnitude and oxygen dependence of G(H_2O_2) reduction

The percentage reduction analysis confirms the trends seen in the time-domain and dose-domain plots. Across all conditions:

- UHDR reduces G(H_2O_2) relative to CONV by approximately 8%–30%.
- Reductions increase with dose due to the quadratic scaling of recombination.
- Reductions are systematically larger at 0.5% O_2, reflecting stronger transient oxygen depletion.
- Multipulse delivery mitigates reductions by allowing chemical recovery between pulses.

These observations are consistent with both diffusion-kinetic simulations and established experimental radiolysis literature [2, 8].

7 Conclusion

This project simulated the effect of pulse duration, instantaneous dose rate, and oxygenation on early water radiolysis under UHDR irradiation. The results demonstrate that UHDR delivery alters the chemical stage of radiolysis in a manner that is quantitatively dose-dependent, oxygen-dependent, and strongly influenced by temporal pulse structure.

Short, high-dose-rate pulses increase spur overlap and enhance radical-radical recombination, leading to suppressed G-values of key molecular products such as H_2O_2. These effects become more pronounced at higher doses and at low oxygen concentrations, where transient oxygen depletion further modifies reaction pathways. In contrast, distributing the same total dose into multiple short pulses reduces these chemical perturbations by allowing partial recovery between pulses.

The findings confirm that the temporal structure of irradiation not only the macroscopic dose rate plays a central role in determining the radiolytic chemical environment under UHDR conditions. These insights provide a mechanistically grounded foundation for connecting radiolysis chemistry to potential biological outcomes in FRT and offer a validated framework for future modelling studies.

Acknowledgments

I would like to sincerely thank my project supervisor for always being available when I needed guidance, for explaining complex concepts in a way I could understand, and for

supporting me throughout this learning journey. I would also like to thank my supervisors from my home university for their encouragement and continued support. Finally, I am grateful to the INTEREST programme organisers for this wonderful initiative, which fosters growth, development, and collaboration.

References

[1] A. Baeyens et al. *Basic Concepts of Radiation Biology.* Springer, Cham, 2023.

[2] G. V. Buxton, C. L. Greenstock, W. P. Helman, and A. B. Ross. Critical review of rate constants for reactions of hydrated electrons, hydrogen atoms and hydroxyl radicals ($\cdot$oh/$\cdot$o$^-$) in aqueous solution. *Journal of Physical and Chemical Reference Data*, 17(2):513–886, 1988.

[3] F. Chappuis, H. N. Tran, P. G. Jorge, et al. Investigating ultra-high dose rate water radiolysis using the Geant4-DNA toolkit and a Geant4 model of the Oriatron ert6 electron linac. *Scientific Reports*, 14:15762, 2024.

[4] J. Ramos-Méndez, J. Perl, J. Schuemann, et al. A review of recent developments in radiobiology modelling using Geant4-DNA. *Physica Medica*, 108:102566, 2023.

[5] S. Incerti, G. Baldacchino, M. Bernal, et al. The Geant4-DNA project. *International Journal of Modeling, Simulation, and Scientific Computing*, 1(2):157–178, 2010.

[6] S. Incerti et al. Geant4-DNA: Overview and recent developments. *International Journal of Radiation Biology*, 96(12):1522–1531, 2020.

[7] S. Agostinelli et al. GEANT4-a simulation toolkit. *Nuclear Instruments and Methods in Physics Research Section A*, 506(3):250–303, 2003.

[8] J. W. T. Spinks and R. J. Woods. *An Introduction to Radiation Chemistry.* Wiley, 1990.

[9] Jay A. LaVerne. Oh radicals and oxidizing products in the gamma radiolysis of water. *Radiation Research*, 153(4):487–493, 2000.

[10] S. M. Pimblott and J. A. LaVerne. Effects of track structure on the ion radiolysis of water. *Journal of Physical Chemistry A*, 106(41):9390–9394, 2002.